Metallographic analysis of Cu–Zr–Al bulk amorphous alloys with yttrium addition

J. Chen [a], Y. Zhang [a,*], J.P. He [a], K.F. Yao [b], B.C. Wei [c], G.L. Chen [a]

[a] State Key Laboratory for Advanced Metals and Materials, University of Science and Technology Beijing, Beijing 100083, China
[b] Department of Mechanical Engineering, Tsinghua University, Beijing 100084, China
[c] Institute of Mechanics, Chinese Academy of Science, Beijing 100080, China

Abstract

Minor yttrium addition can improve the glass-forming ability of Cu–Zr–Al ternary alloys via suppression of the growth of eutectic clusters. Yttrium addition also makes the room temperature ductility of the alloys decrease, and both the compressive strength and elastic strain limits increase slightly.
© 2006 Acta Materialia Inc. Published by Elsevier Ltd. All rights reserved.

Keywords: Casting; Copper alloys; Amorphous materials; Microstructure; Solidification

1. Introduction

Recently, bulk amorphous alloys (BAA) have attracted a great deal of attention because they exhibit unique properties compared with their counterpart crystalline materials, e.g., they have 2–3 times the fracture strength of crystalline materials [1], high elastic strain limit, and high corrosion resistance [1–3]. However, exploring the new kinds of bulk amorphous alloys has been a challenge up to now. Some researchers found that the minor addition of rare earth metals can greatly improve the glass-forming ability (GFA) of the alloys, e.g., Zr–Al–Ni–Cu–Y, Mg–Cu–Gd, Fe–TM–B–Y, Fe–B–Y [4–7]. Establishing the mechanism of Y addition in the formation of BAAs would also mean a breakthrough in developing new BAAs. It is proposed that possible mechanisms are: (i) Y improves the manufacturability of the alloys by scavenging the oxygen impurity via the formation of innocuous yttrium oxides and reduces heterogeneous nucleation [4–6]; (ii) Y adjusts the compositions closer to the eutectic and thus lowers the liquidus temperature [8]; (iii) Y, with its large atom size, could destabilize the competing crystalline phase, by alloying with metastable phases forms upon devitrification, e.g., Fe–Cr–Mo–Y–C–B [9]. In this paper, a metallographic method was used to study the mechanism of the yttrium effect in improving GFA; for simplicity, a CuZrAl ternary alloy system was selected.

2. Experimental

The master alloys were prepared by arc melting the constituent elements—Cu, Zr, Al and Y with purities of 99.95%, 99.99%, 99.7% and 99.9%, respectively—in a Ti-gettered high-purity argon atmosphere. Their nominal compositions are $(Cu_{0.48}Zr_{0.48}Al_{0.04})_{100-x}Y_x$ ($x = 0$, 1, 2), and each ingot was melted at least three times in order to obtain chemical homogeneity. The ingots were then remelted under high vacuum (10^{-4} Pa) and cast by suction of the melt into a copper mold to obtain 50 mm-long cylindrical rods of 3 mm in diameter, denoted by S01($x = 0$), S11($x = 1$), S21($x = 2$). The structure of the as-cast samples

* Corresponding author. Tel./fax: +86 010 62322160.
  E-mail address: drzhangy@skl.ustb.edu.cn (Y. Zhang).

(transverse cross-sections) was characterized by X-ray diffraction (XRD) using a MXP21VAHF diffractometer with Cu Kα radiation. Differential scanning calorimetry (DSC) was carried out in a NETZSCH STA 409C at a heating rate of 10 K/min to 900 °C. Cylindrical samples were prepared by sparking, cut to 6 mm in length. The compression tests were carried out using three or four of the samples. Some of the samples were polished and etched by hydrofluoric acid, then sulfuric acid and sodium dichromate liquor. The fracture surface and the etched samples were studied by scanning electron microscopy (SEM).

3. Results and discussion

Fig. 1 shows the XRD patterns of $(Cu_{48}Zr_{48}Al_4)_{100-x}$-$Y_x$, ($x = 0$, 1, 2) rod samples with diameter of 3 mm denoted S01 ($Cu_{48}Zr_{48}Al_4$), S11 (($Cu_{0.48}Zr_{0.48}Al_{0.04})_{99}Y_1$) and S21 (($Cu_{0.48}Zr_{0.48}Al_{0.04})_{98}Y_2$), respectively. It can be seen that S01 is a mixture of a small amount of crystalline and amorphous material, while S11 and S21 are fully amorphous. Because there is texture formed along the specific crystal direction, only two strong crystal peaks are observed. The two peaks agree well with CuZr phase. The ternary Cu–Zr–Al diagram phase with 4 at.% Al could be projected on the Cu–Zr binary phase diagram. According to the binary phase diagram of Cu–Zr, the system with 48 at.% of Zr (as shown in Fig. 2 marked by S) could precipitate CuZr phase as the primary phase, and a mixture of CuZr and $Cu_{10}Zr_7$ as binary eutectic. The high cooling rate of copper mold casting may lead to the eutectic coupled zone being skewed towards the primary phase with higher slope of liquidus line, and also the optimum glass formation being shifted to the off-eutectic [10]. It has been reported that $Cu_{48}Zr_{48}Al_4$ alloy can be cast into 5 mm diameter amorphous rod [11]; however, we could not form a fully amorphous rod sample of 3 mm, which may be due
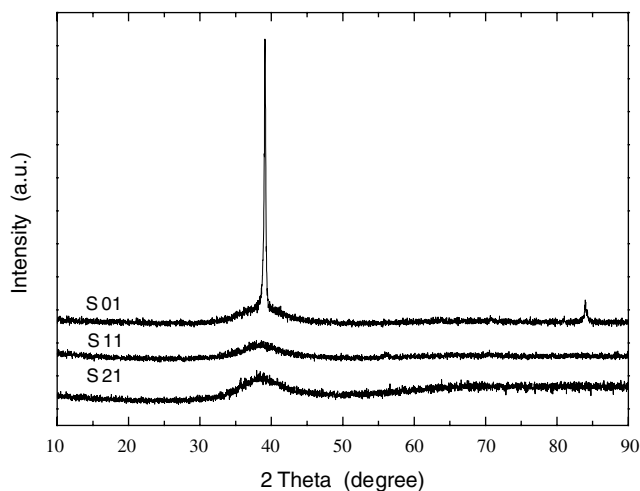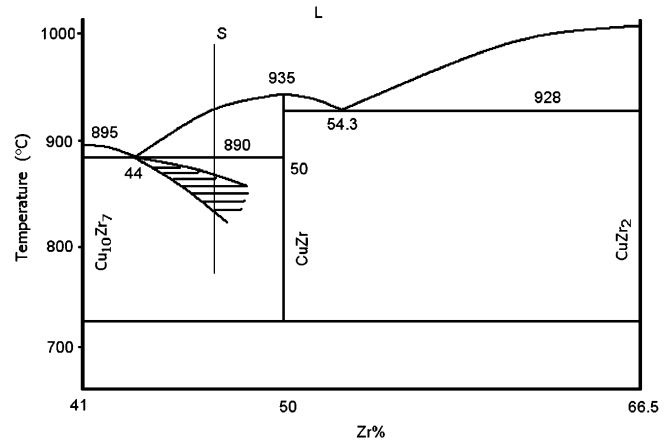

Fig. 2. Phase diagram of Cu–Zr system with the Zr content range 41–66.5 at.%.

to the manufacturability of the alloys not being good enough. With 1 at.% yttrium addition, at least 3 mm amorphous rod can be formed.

Fig. 3 shows the SEM secondary electron images of S01, S11, and S21 after polishing and etching. It can be seen that etching made the amorphous surface split, and after etching, there is more apparent contrast on the partially amorphous surface (Fig. 3(a)) than on the fully amorphous (Fig. 3(d) and (f)). The etched surface can be divided into three areas: planes 1 and 2 without any contrast are amorphous phase, and rough area 3 is composed of circles with contrast and different diameters. In some circles of area 3, there are cross-like precipitates in the center as shown in Fig. 3(b). The cross precipitate is the primary dendrite phase. Fig. 3(c) is an image of the edge of the circle: the outer is very flat which is amorphous, while the inner is laminar like crystalline, which is a eutectic cluster. Compared with Fig. 3(a), the flat areas are larger and more continuous in Fig. 3(d), most of the rough circles become smaller (Fig. 3(e)), and the cross precipitate phases in the center emerge in most circles. But in Fig. 3(f), the circles and the cross precipitate phases have disappeared, and there are only some irregular splits (Fig. 3(g)) and some bulges about to split (Fig. 3(h)).

Fig. 3 illustrates that the microstructure of the alloys varies with increasing yttrium addition. With 1 at.% Y addition, the size of the eutectic clusters decreases and the amount of the cross precipitate increases; this implies that minor yttrium addition can suppress the growth of the eutectic cluster, and facilitate the nucleation of the primary phase. With 2 at.% Y addition, both the eutectic cluster and the primary dendrite phases have disappeared. This indicates that further addition of yttrium can suppress both the precipitation of the cross phase and the growth of the eutectic.

Fig. 4 is a schematic time–temperature-transformation (TTT) curve of the alloy to explain the unique microstructure with Y addition. It illustrates the variation of the

Fig. 1. XRD patterns of the rod samples with diameter of 3 mm: S01 ($Cu_{48}Zr_{48}Al_4$), S11 (($Cu_{0.48}Zr_{0.48}Al_{0.04})_{99}Y_1$) and S21 (($Cu_{0.48}Zr_{0.48}Al_{0.04})_{98}Y_2$).
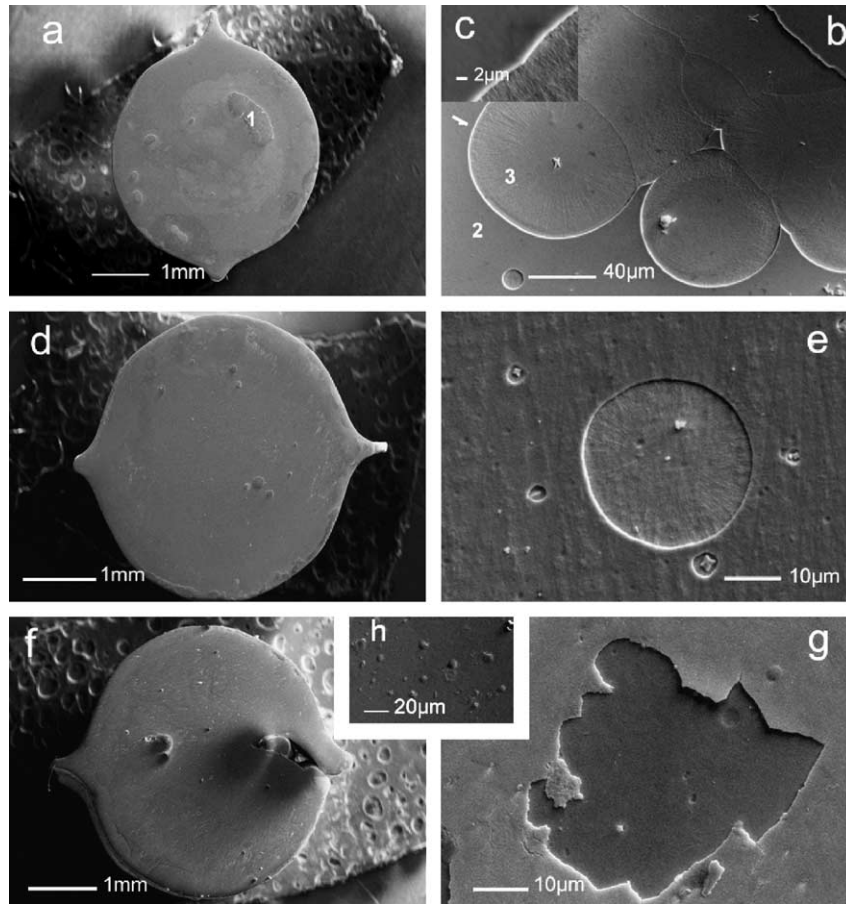
Fig. 3. SEM secondary electron images of S01 (a)–(c), S11 (d) and (e), and S21 (f) and (g) after polishing and etching.
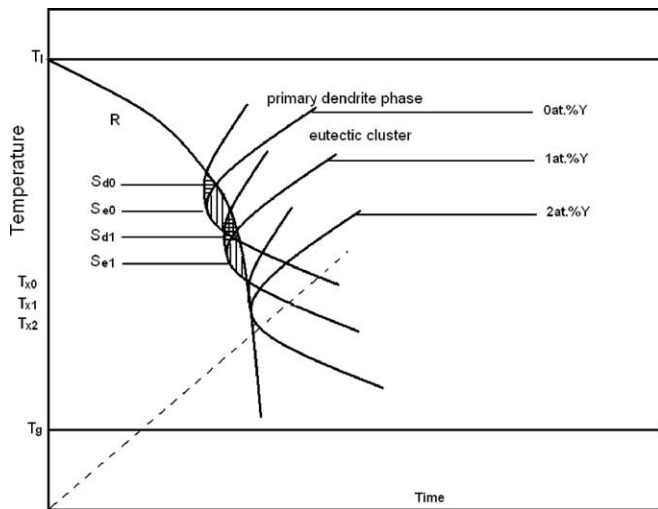

Fig. 4. Schematic temperature–time-transformation (TTT) diagram of the alloys with Y additions.

eutectic and the primary dendrite phases. It shows that the TTT curve moves as the amount of Y varies. A minor addition of Y could reduce the heterogeneous nucleation [4–6,9] and prolong incubation period, so the TTT curve moves to the right when Y content increases. When heated at a certain rate, the amorphous begins to crystallize at the temperature of T_x, which is shown as the cross point of the dashed line and the TTT curves. In Fig. 5 the T_x of S01, S11 and
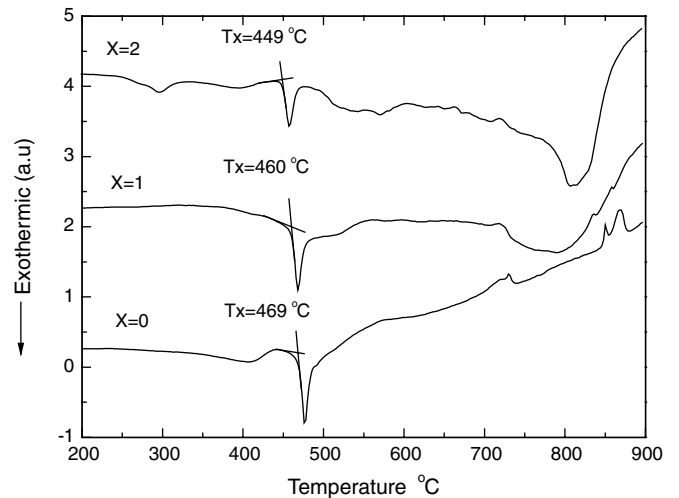

Fig. 5. DSC traces of the rod samples of S01 ($x = 0$), S11 ($x = 1$) and S21 ($x = 2$); the T_x of S01, S11 and S21 are 469, 460 and 449 °C, respectively.

S21 are 469, 460 and 449 °C, respectively; the decreasing tendency indicates that the TTT curve moves downwards.

The area of intersection of primary dendrite phase with the cooling curve marked S_d (S_{d0}, S_{d1} with transverse lines shown in Fig. 4), and of eutectic cluster marked S_e (S_{e0}, S_{e1} shown in Fig. 4 vertically). As the TTT curve moves, S_e decreases ($S_{e0} > S_{e1}$) so that the growth of the eutectic cluster was suppressed; S_d increases at first ($S_{d0} < S_{d1}$) and then decreases (with no intersection) as shown in Fig. 3, so the amount of the primary dendrites increases when yttrium addition is 1 at.%, then decreases when yttrium addition is 2 at.%.

Fig. 6 shows the stress–strain curves of S01, S11 and S21. It is noticed that the alloy S01 exhibits distinct plastic elongation of 5.32%, while S11 exhibits 0.85 % plastic strain. The Young's modulus (E), yield strength σ_y, compressive strength σ_{max}, elastic strain limit ε_e and plastic strain limit ε_p are listed in Table 1. The Y addition makes ε_p decrease, and the compressive strength and ε_e increase slightly. Before the end of the stress–strain curve of S01 there is apparently serrated flow, which also can be seen partially on S11. The stress fluctuation is the distinct evidence of the formation and propagation of multiple shear bands. The increasing stress activates one shear band and the shear band slides so that the stress decreases. When the sliding shear band is hindered, the stress has to increase again, and a new shear band nucleates and propagates to decrease the stress again before it is blocked. It can also be confirmed in Fig. 7, which shows multiple shear bands on specimen surface of S01 and S02. On cylindrical S01 rod the shear bands with closer spacing of 1–2 μm (Fig. 7(a) and (b)) can be easily found, while on S11 the shear bands spacing increases. There are some single shear bands on the S21 rod surface instead of the shear band cluster.

Fig. 8 shows the fracture surfaces of S01 (a) and (b), S11 (c) and (d), and S21 (e); the typical fracture surface consists of a well-developed vein pattern of bulk glassy alloys. In Fig. 8(a) and (b), the vein patterns are arranged with different denseness, and the undersized vein patterns are crowded, which indicates the shear band may pass at a slower velocity. The vein pattern in Fig. 8(c) shows appar-
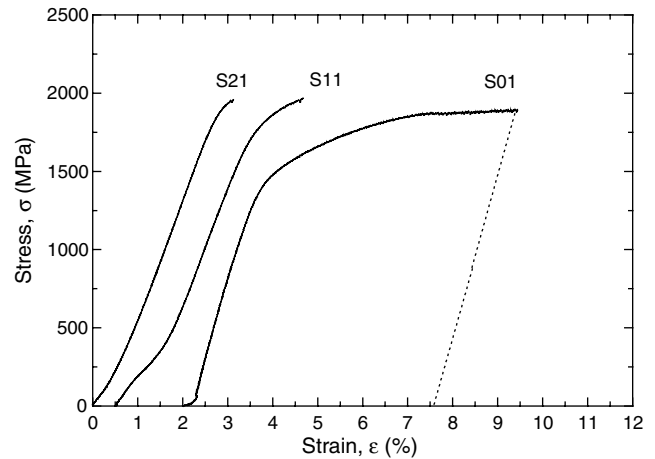
Fig. 6. Typical compressive stress–strain curves of S01, S11, and S21 rods with diameters of 3 mm.

Table 1
Room temperature compressive properties of S01, S11 and S21 alloys

Alloy	E (GPa)	σ_y (MPa)	σ_{max} (MPa)	ε_e (%)	ε_p
S01	102.80	1198.5	1882.3	2.204	5.316
S11	87.29	1563.7	1865.8	3.029	0.851
S21	75.48	1844.6	1981.0	2.900	0.284

Young's modulus (E), yield stress (σ_y), compressive strength (σ_{max}), elastic strain limit (ε_e) and plastic strain (ε_p).

ent directionality. Compared with Fig. 8(a) and (d), there are more flat areas in Fig. 8(e). The flat area are formed by the expedite slip of shear bands, thus the increase of the flat area means less hindrance to shear bands and less plastic deformation.

The feasible hindrance of the shear bands in S01 is the crystalline phase in it; the sliding shear bands are blocked and multiple shear bands start. The undersized dimple-like vein pattern also indicates that the shear bands slide by at a slower velocity. So S01 exhibits distinct plastic elongation with $\varepsilon_p = 5\%$. There is more amorphous material in S11 and S21, while less hindrance to shear bands, and less plastic elongation.
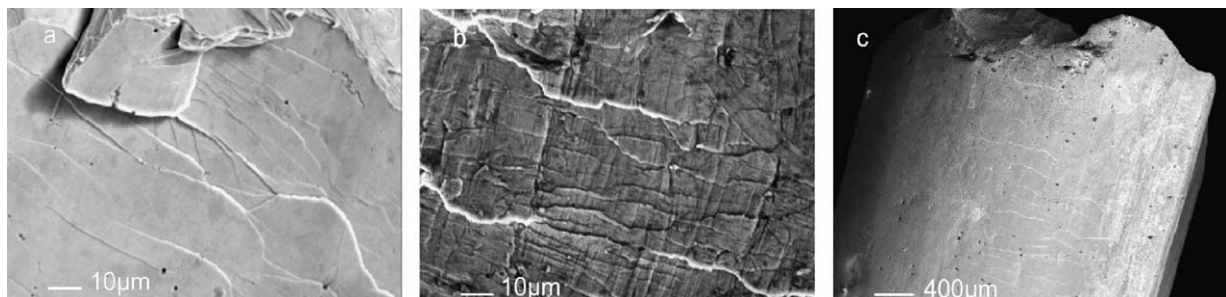

Fig. 7. SEM images of shear bands on surfaces of S01 (a) and (b) and S11 (c) specimens.
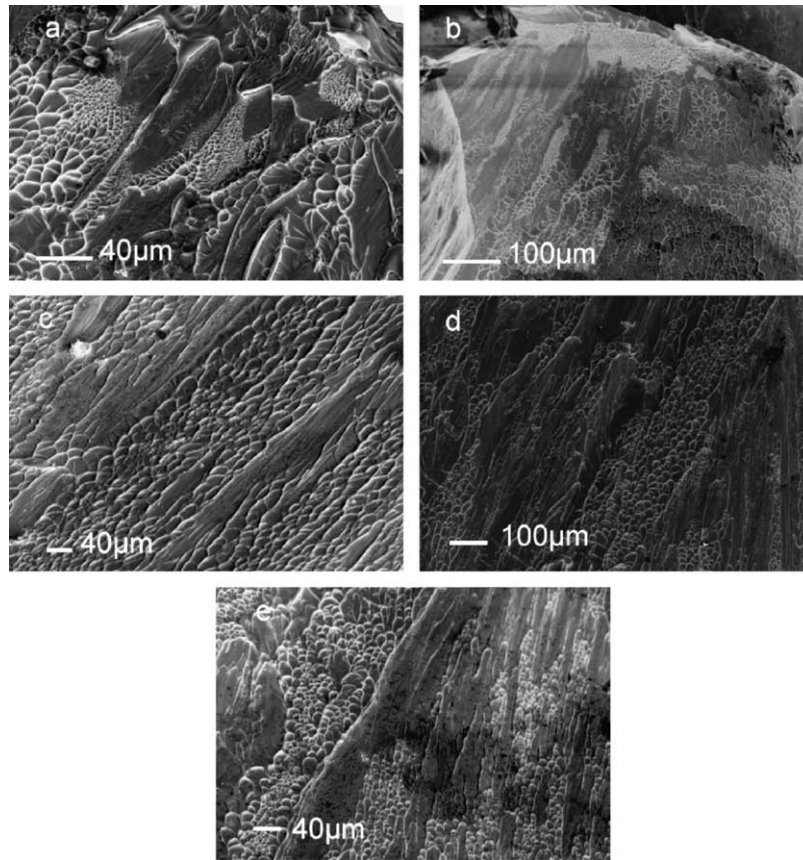
Fig. 8. SEM images of fracture surface of S01 (a and b), S11 (c and d) and S21 (e).

4. Conclusions

In summary, a minor addition of yttrium (1–2%) can markedly improve the manufacturability of $Cu_{48}Z_{48}Al_4$ alloy. The mechanism of the positive effect is via the suppression of the growth of eutectic clusters with less Y addition, and via the suppression of both the growth of eutectic clusters and the precipitation of the primary dendrite phase for 2% Y addition; this is shown to be theoretically feasible by the discussion of the TTT curve. The Y addition also makes the ε_p of the alloys decrease, and both the compressive strength and ε_e increase slightly. The fracture surface of the alloys has typical vein patterns, and the flat areas of the vein pattern increase with Y addition. Although it is concluded that Y enhances the GFA of the CuZrAl alloy by suppressing the growth of the eutectic cluster and the precipitate of the primary dendrite phase, the mechanism still needs further study.

Acknowledgements

References

[1] Inoue A. Mater Sci Eng A 2000;375–377:16.
[2] Wang WH, Dong C, Shek CH. Mater Sci Eng R 2004;44(2–3):45.
[3] Johnson WL. MRS Bull 1999:42.
[4] Zhang Y, Pan MX, Zhao DQ, Wang RJ, Wang WH. Mater Trans JIM 2002;41(11):1410.
[5] Lu ZP, Liu CT, Porter WD. Appl Phys Lett 2003;83(13):9.
[6] Xi XK, Wang RJ, Zhao DQ, Pan MX, Wang WH. J Non-Cryst Solids 2004;344:105.
[7] Zhang J, Tan H, Feng YP, Li Y. Scripta Mater 2005;53:183.
[8] Xu DH, Duan G, Johnson WL. Phys Rev Lett 2004;92:245.
[9] Ponnambalam V, Poon SJ, Shiflet GJ. J Mater Res 2004;19:1320.
[10] Zhang Y, Xu W, Tan H, Li Y. Acta Mater 2005;53:2607.
[11] Yu P, Bai HY, Tang MB, Wang WL. J Non-Cryst Solids 2005;351:1328.